Self-assembly of a colloidal interstitial solid solution with tunable sublattice doping: Supplementary information

L. Filion,* M. Hermes, R. Ni, E. C. M. Vermolen,† A. Kuijk, C. G. Christova,‡
J. C. P. Stiefelhagen, T. Vissers, A. van Blaaderen, and M. Dijkstra
Soft Condensed Matter, Debye Institute for NanoMaterials Science,
Utrecht University, Princetonplein 1, NL-3584 CC Utrecht, the Netherlands

I. CRYSTAL STRUCTURE LS_6

In the main paper we use full free-energy calculations to determine the phase diagram for binary mixtures of hard spheres with size ratio $\sigma_S/\sigma_L = 0.3$ where $\sigma_{S(L)}$ is the diameter of the small (large) particles. The phases we considered included a structure with LS_6 stoichiometry for which we could not identify an atomic analogue. Snapshots of this structure from various perspectives are shown in Fig. S1.

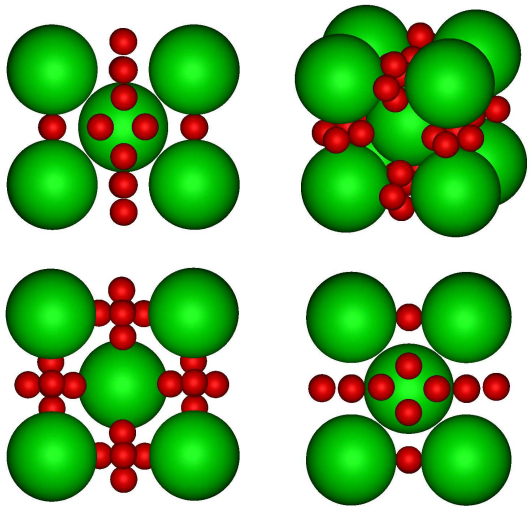

FIG. S1: Unit cell of the binary LS_6 superlattice structure described in this paper. Note that both species exhibit long-range crystalline order. The unit cell is based on a body-centered-cubic cell of the large particles in contrast to the face-centered-cubic cell associated with the interstitial solid solution covering most of the phase diagram (Fig. 1).

II. PHASE DIAGRAM AT CONSTANT VOLUME

In the main paper, we present the $x_S - p$ representation of the phase diagram where $p = \beta P \sigma_L^3$ is the reduced pressure, $x_S = N_S/(N_S + N_L)$, $N_{S(L)}$ is the number of small (large) hard spheres, $\beta = 1/k_B T$, k_B is the Boltzmann constant, and T is the absolute temperature. This is the natural representation arising from common tangent constructions at constant pressure and the representation required for further simulation studies such as nucleation studies. However, experimentally other representations are often useful. In particular, in experiments it is often simpler to know the partial packing fractions of the various particle species and as a result constant volume representations are often the more natural representation when comparing predicted phase behaviour to that found experimentally. In

*Presently: Department of Chemistry, University of Cambridge,Lensfield Road, Cambridge, CB2 1EW, United Kingdom
†Presently: Shell Projects and Technology, Kessler Park 1, NL-2288 GS Rijswijk, the Netherlands
‡Presently: PTG/e BV, Het Kranenveld (MA 1.11), P.O. Box 6284, 5600 HG Eindhoven, The Netherlands

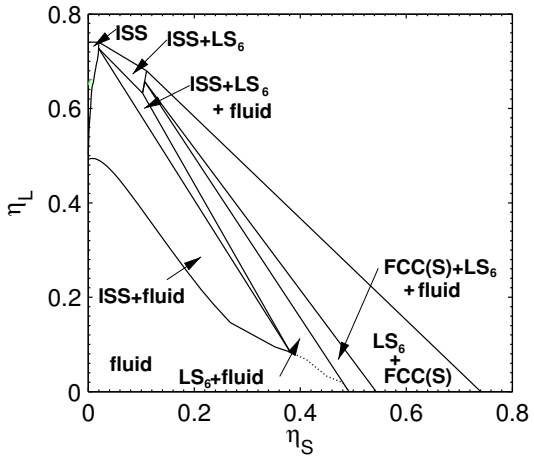

FIG. S2: Phase diagram in the η_S-η_L representation. The dotted line indicates a large uncertainty in the phase boundary.

Fig. S2 we present the phase diagram in the small particle volume fraction-large particle volume fraction ($\eta_S - \eta_L$) representation, where $\eta_{S(L)} = \pi\sigma^3_{S(L)}/6V$ is the small (large) sphere volume fraction, and V is the volume.

III. SEDIMENTATION

In the main paper we have discussed the experimental realization of an ISS phase in sedimentation experiments of core-shell silica particles. In Fig. S3 we present two more example confocal images of the interstitial solid solution phase, one with $n \simeq 0.1$ and one with $n \simeq 0.8$ as well as a larger confocal image of the system shown in Fig. 2. The experiments were performed with large 1.4 μm core shell silica colloids. The core was dyed with fluorescein isothiocyanate (FITC) and the core diameter was 0.4 μm [1]. The small colloids had a rhodamine isothiocyanate (RITC) dyed core with a diameter of 0.37 μm and a total diameter of 0.42 μm [2]. The large colloids had a polydispersity of 2% and the small colloids a polydispersity of 7%. The solvent was an index matched mixture of 80% (volume percent) dimethylsulfoxide (DMSO) and water. The size of the domains was increased using an AC electric field of 100 $V/$mm which was removed after the particles had sedimented.

IV. DIFFUSION OF SMALL PARTICLES

In the main paper we discuss the diffusion of the small particles. The mean square displacement $\left\langle \Delta r_S^2(t) \right\rangle = \left\langle \left(r_S(t) - r_S(0)\right)^2 \right\rangle$ of the small particles displays a subdiffusive regime characteristic of caging which increases as the number density of the large particles $\rho_L\sigma_L^3$ increases. Here $r_S(t)$ denotes the small particle coordinate at time t. In Fig. S4 we show this subdiffusive regime for an ISS with stoichiometry $n = 0.5$ and varying $\rho_L\sigma_L^3$. From the mean square displacement we can determine the long-time self-diffusion coefficient. In the main paper in Fig. 3, we plot the long-time self-diffusion as a function of number density of the large particles ($\rho_L\sigma_L^3$). Surprisingly we find that the diffusion coefficient increases as we increase the ISS stoichiometry at fixed ρ_L. To explore possible explanations for this behaviour, we calculate the mean square deviation of the large particles from their ideal lattice sites $\left\langle (\Delta r_L(t))^2 \right\rangle = \left\langle (\mathbf{r}_L(t) - \mathbf{r}_L^{\rm id})^2 \right\rangle$ as a function of stoichiometry n of the ISS (Fig. S5), where $\mathbf{r}_L^{\rm id}$ denotes the ideal lattice positions of the large particles. We find the mean square displacement increases upon increasing the stoichiometry n. We suspect that this arose due to an increase in the depletion potential between the large particles as a function of n. The increase in the mean square displacement results in more space for the small particles to diffuse. As a consequence, the free-energy barrier heights decrease with stoichiometry n of the ISS as shown in Fig. 3 which explains the increase in the long-time self-diffusion coefficient of the small particles with increasing n as shown in Fig. 3.

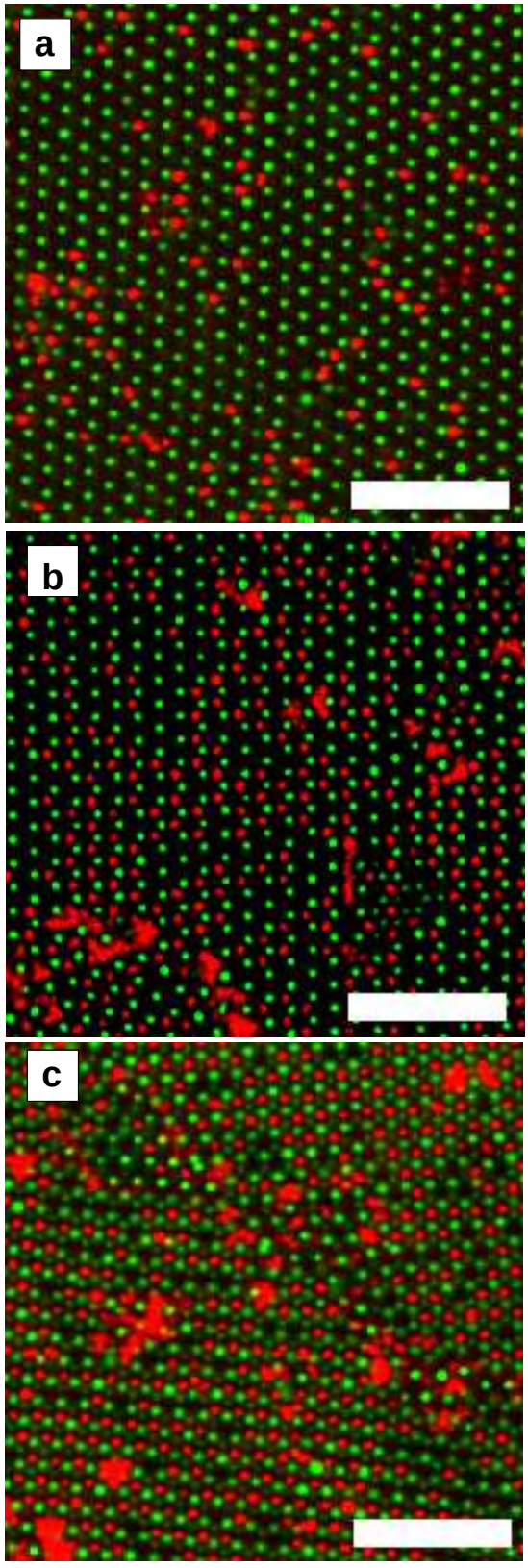

FIG. S3: Confocal images of an interstitial solid solution with size ratio $q = 0.3$ for various stoichiometries $n \simeq$ **a** 0.1, **b** 0.3, and **c** 0.8. In these images two (111) planes of the crystal, one consisting of mostly small (red) particles with the other consisting of mostly large (green) particles have been overlayed in order to be viewable in the same figure. The larger and darker red regions correspond to defects, such as vacancies, in the underlying lattice of green particles which have been filled by many small (red) particles. Scale bars are 10 μm.

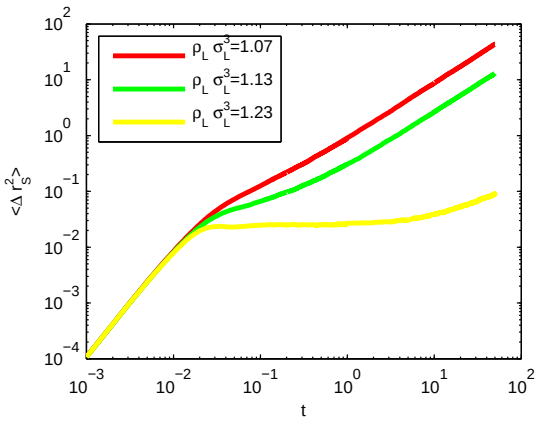

FIG. S4: Caging of small particles in an interstitial solid solution. Using event driven MD simulations with $N_L = 256$ large particles and stoichiometry $n = 0.5$ we measured the mean square deviation $\langle \Delta r(t)_S^2 \rangle = \langle (\mathbf{r}_S(t) - \mathbf{r}_S(0))^2 \rangle$ of the small particles as a function of time for various number densities of the large particles ρ_L. Note that $r_S(t)$ denotes the small particle coordinate at time t. Here we plot the $\langle \Delta r_S(t)^2 \rangle$ vs time (in MD units) on a log-log scale. As ρ_L increases the subdiffusive regime also increases.

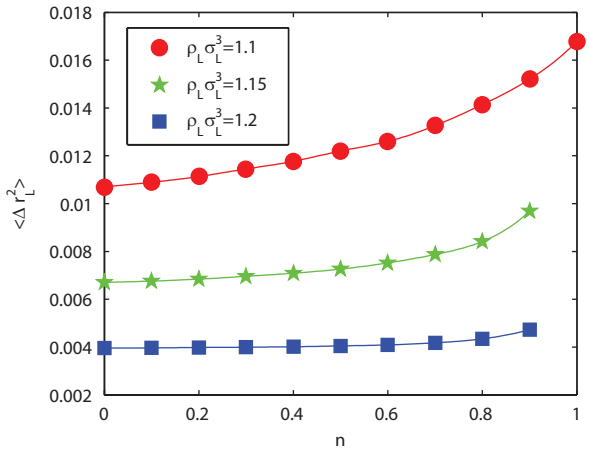

FIG. S5: Mean square deviation of large particles from their ideal lattice sites as a function of ISS stoichiometry n for large particle number densities ρ_L as labelled. The mean square deviations, $\langle (\Delta r_L(t))^2 \rangle = \langle (\mathbf{r}_L(t) - \mathbf{r}_L^{\rm id})^2 \rangle$ with $\mathbf{r}_L^{\rm id}$ the ideal lattice positions of the large particles, were determined using a Monte Carlo simulation with $N_L = 864$ large particles and correcting for the center of mass motion of the large particles.

V. AN INTERSTITIAL SOLID SOLUTION IN AN OPPOSITELY CHARGED PARTICLE MIXTURE

The interactions between colloidal particles is generally quite complicated, consisting of e.g. van der Waals interactions between the cores, a steric stabilizer on the surface, charges on the particles and in the solvent, and depletion effects due to smaller particles present in the solvent. While systems can often be constructed where these interactions are mostly screened and the particles behave like hard-core particles, it is also important to know whether an interstitial solid solution could be present in other colloidal systems where interactions aside from the hard core play a role. To explore this possibility we examined the sedimentation profile of a binary mixture of oppositely charged colloids. As demonstrated in Figures S6 and S7, this system also appears to exhibit an interstitial solid solution phase. Hence, we conclude that the ISS phase is not specific to hard spheres, but is likely present in a wide variety of colloidal and nanoparticle mixtures.

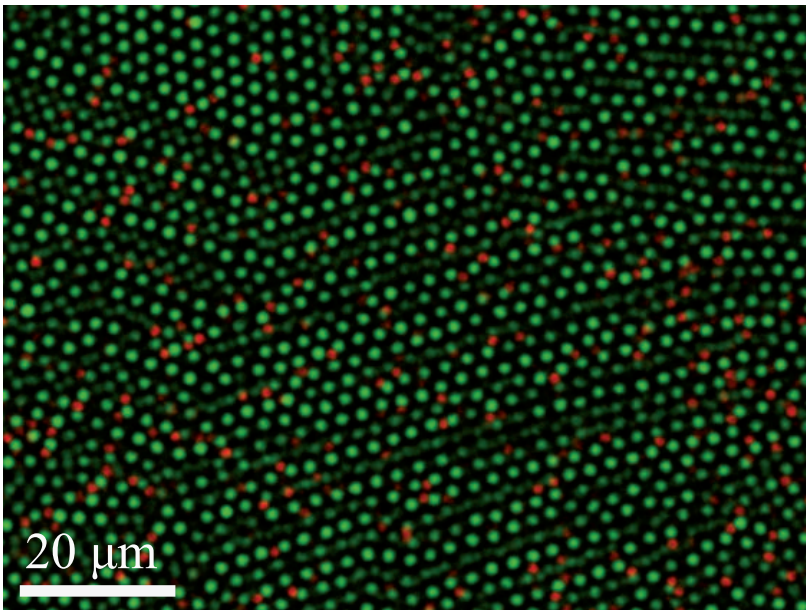

FIG. S6: Typical confocal image of the ISS structure found in a binary system of oppositely charged PMMA particles with size ratio σ_S/σ_L=0.73 dispersed in a mixture of 23.7 w% cis-decahydronaphthalene and 76.3 w% cyclohexylbromide. The colloids were sterically stabilised to prevent short-range Van der Waals attractions. The large (green) and small (red) particles have a diameter 1.88 μm (polydispersity 3 %) and 1.37 μm (polydispersity 5 %) respectively. The overall packing fraction was $\eta = 0.2$. The large particles mutually repel each other and formed a crystal lattice. The small particles were found on random positions in between the lattice. See Fig. S7 for more details.

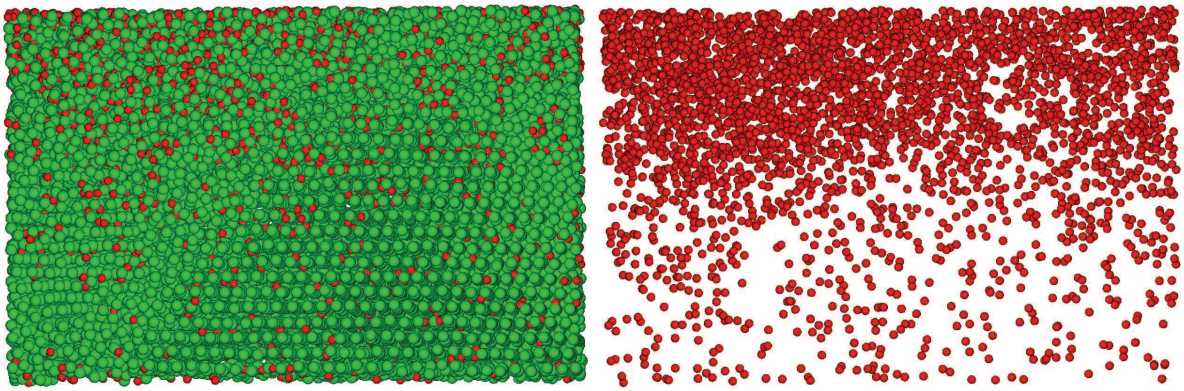

FIG. S7: 3-D reconstruction of an interstitial solid solution in a binary mixture of oppositely charged colloids. Left: Rendered 3-D reconstruction from a stack of 244 confocal images with a spacing of 0.25 μm between them corresponding to the system described in Fig. S6. We identified a face-centred-cubic-lattice of the mutually repelling large particles with a lattice parameter for the cubic unit cell of $a \approx 3.8$ μm. In the lower part of the sample an ISS was formed with a fluid on top of it. Whereas the large particles do not touch each other, the small particles were found to stick to one or more large particles in the lattice. This, in addition to the observation that the small particles do not appear to occupy a position on the lattice of the large particles, demonstrates that the large and small particles were oppositely charged. Right: The same 3-D reconstruction showing only the small particles in the fluid (top) and the ISS (below). We note that in sequential confocal images, some of the small particles were observed hopping from one interstitial site to another.

[1] Hoogenboom, J. P., Vergeer, P. & van Blaaderen, A. A real-space analysis of colloidal crystallization in a gravitational field at a flat bottom wall. *J. Chem. Phys.* **119**, 3371 (2003).
[2] Vermolen, E. C. M. *et al.* Fabrication of large binary colloidal crystals with a NaCl structure. *Proc. Nat. Ac. Sci.* **106**,

16063–16067 (2009).